NANO LETTERS
Letter
Cite This: Nano Lett. 2018, 18, 2217−2225
pubs.acs.org/NanoLett

Ultrathin Polypyrrole Nanosheets via Space-Confined Synthesis for Efficient Photothermal Therapy in the Second Near-Infrared Window

Xu Wang,[†] Yinchu Ma,[‡] Xing Sheng,[§] Yucai Wang,*[,‡] and Hangxun Xu*[,†]

[†]Department of Polymer Science and Engineering, CAS Key Laboratory of Soft Matter Chemistry, University of Science and Technology of China, Hefei, Anhui 230026, China

[‡]School of Life Sciences and Medical Center, University of Science and Technology of China Hefei, Anhui 230027, China

[§]Department of Electronic Engineering, Tsinghua University, Beijing 100084, China

Supporting Information

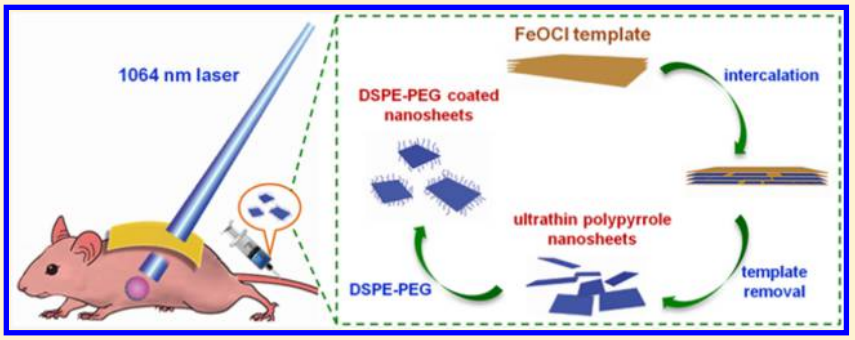

ABSTRACT: Extensive efforts have been devoted to synthesizing photothermal agents (PTAs) that are active in the first near-infrared (NIR) region (650−950 nm). However, PTAs for photothermal therapy in the second NIR window (1000−1350 nm) are still rare. Here, it is shown that two-dimensional ultrathin polypyrrole (PPy) nanosheets prepared via a novel space-confined synthesis method could exhibit unique broadband absorption with a large extinction coefficient of 27.8 L g^{-1} cm^{-1} at 1064 nm and can be used as an efficient PTA in the second NIR window. This unique optical property is attributed to the formation of bipolaron bands in highly doped PPy nanosheets. The measured prominent photothermal conversion efficiency could achieve 64.6%, surpassing previous PTAs that are active in the second NIR window. Both in vitro and in vivo studies reveal that these ultrathin PPy nanosheets possess good biocompatibility and notable tumor ablation ability in the second NIR window. Our study highlights the potential of ultrathin two-dimensional polymers with unique optical properties in biomedical applications.

KEYWORDS: *Polypyrrole, two-dimensional polymer, photothermal therapy, tumor ablation, doping*

Photothermal therapy (PTT) using localized heat generated by light-absorbing agents under near-infrared (NIR) laser radiation is a very promising method for thermal ablation of cancer cells.[1−6] Unlike traditional cancer treatments, PTT is a minimally or noninvasive therapeutic modality, offering distinct advantages such as simple procedures and fast recovery after cancer therapeutics.[7,8] Nanostructured materials with prominent photothermal conversion efficiency (PTCE) are highly desirable for PTT.[9,10] However, developing practical photothermal agents (PTAs) for clinical applications still remains a significant challenge. Ultrathin two-dimensional (2D) nanosheets with intriguing physical and optical properties could potentially offer new solutions to realize efficient PTT with large extinction coefficient and high PTCE.[11−13] To date, various 2D nanomaterials including graphene derivatives, transition-metal dichalcogenides, black phosphorus, MXenes, and metallic nanosheets have been investigated as PTAs for both in vitro and in vivo biomedical studies.[14−21] However, these nanosheet-based PTAs generally absorb NIR light only in the wavelengths ranging from 650 to 950 nm (first NIR window, NIR I).

Compared to the NIR I window, the second NIR window (1000−1350 nm, NIR II) is more appealing for practical PTT as NIR II window could offer more efficient tissue penetration due to reduced photon scattering and much lower tissue background.[22,23] Meanwhile, NIR II window could allow higher maximum permissible exposure (MPE) to laser. The MPE for skin exposure is 1 W cm^{-2} at the NIR II region whereas this value is merely 0.33 W cm^{-2} at 808 nm.[23] Therefore, it is highly desirable to realize efficient PTT in the NIR II window, especially for treating deep-tissue buried tumors. So far, nanomaterials that are known to be active in the NIR II window for PTT are limited to copper sulfide-based hybrid materials,[24,25] gold nanostructures,[26−28] silver nanoplates,[29] carbon nanotubes,[30] graphene-based composite,[31] and large

Received: November 4, 2017
Revised: March 8, 2018
Published: March 12, 2018

DOI: 10.1021/acs.nanolett.7b04675
Nano Lett. 2018, 18, 2217−2225

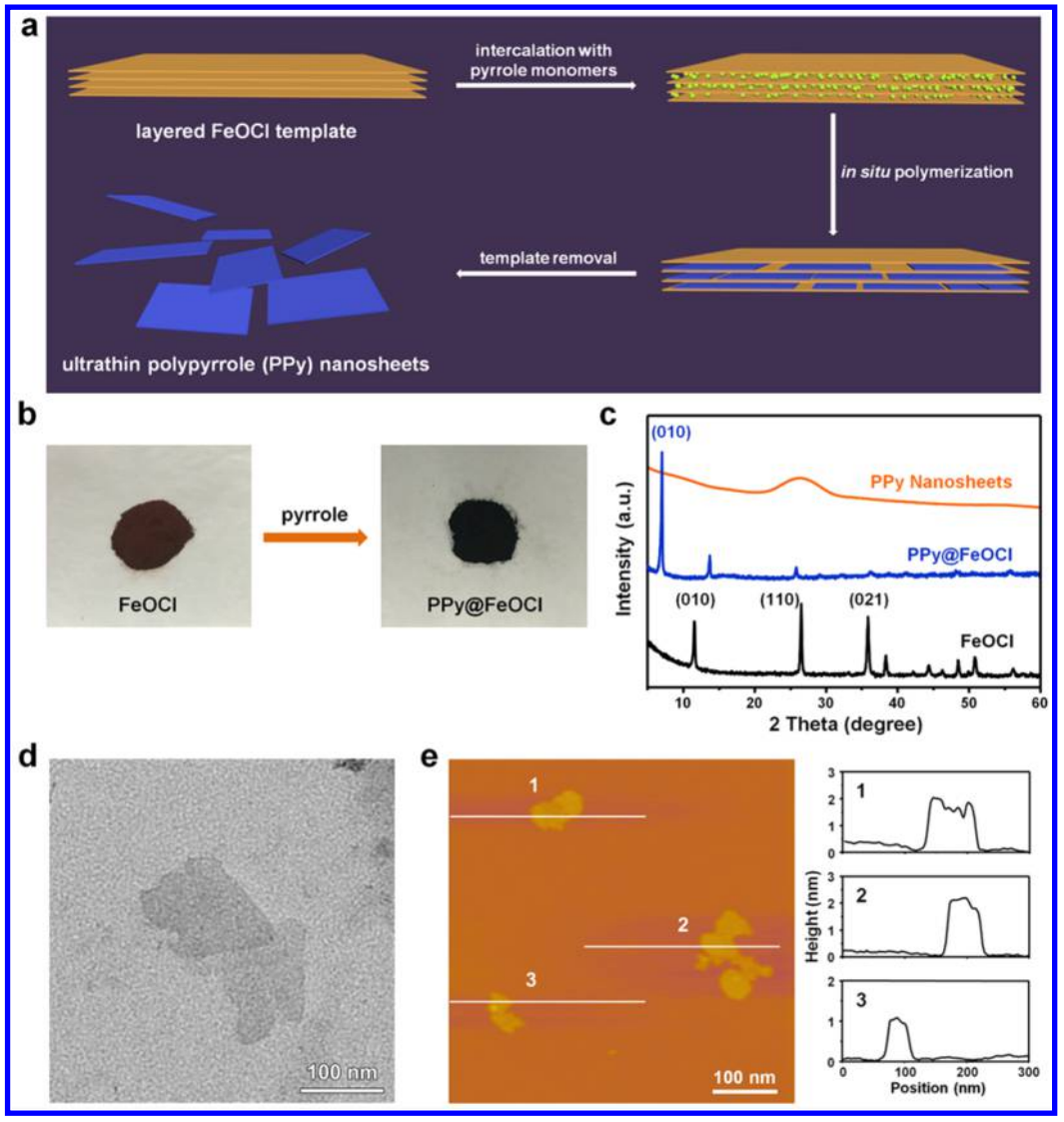

Figure 1. (a) Schematic illustration of the process for synthesizing ultrathin PPy nanosheets using a space-confined synthesis method. During acid washing to remove the FeOCl template, Cl^- ions are doped into the PPy nanosheets. (b) Photographs of the layered FeOCl template before (left) and after (right) intercalating and polymerizing with pyrrole monomers. (c) Powder X-ray diffraction patterns of layered FeOCl template, FeOCl template intercalated with PPy, and as-synthesized PPy nanosheets. (d) TEM image of the ultrathin PPy nanosheets. (e) AFM image and corresponding height profiles of the ultrathin PPy nanosheets.

conjugated polymer particles.[32] To the best of our knowledge, 2D polymer nanosheets with suitable absorbance in NIR II window for PTT have not been reported so far.

Polypyrrole (PPy) is a promising low-cost PTA with good biocompatibility, low cytotoxicity, high photostability, and excellent light-to-heat conversion performance.[33] Unfortunately, previous studies primarily focus on employing PPy nanoparticles for PTT in the NIR I region.[34−40] The potential of PPy for PTT in the NIR II window has been largely neglected and not been exploited yet. In fact, the electronic structures and associated optical properties of PPy can be finely tuned via controlled doping process.[41−44] With increased doping levels, polaron and bipolaron bands could appear in the band gap of PPy and therefore cause strong absorbance in the NIR II region.[42,43] In this context, we surmise that properly doped ultrathin PPy nanosheets with suitable lateral size (~100 nm) should be an ideal candidate for PTT in the NIR II window as the ultrathin planar structure is very convenient for achieving high-level doping in PPy nanostructures. To obtain ultrathin PPy nanosheets, we first developed a space-confined approach using a layered inorganic template to synthesize ultrathin PPy nanosheets. The as-synthesized PPy nanosheets exhibit unique absorption in both NIR I and NIR II windows and could be easily coated with 1,2-distearoyl-*sn*-glycero-3-phosphoethanolamine-*N*-[methoxy(polyethylene glycol)-2000] (DSPE-PEG) to obtain highly stable physiological dispersions for biomedical applications. Notably, the PPy nanosheets reported here possess a large extinction coefficient (27.8 L g^{-1} cm^{-1}) and high PTCE (64.6%) at 1064 nm, which is the highest among the reported PTAs in the same spectral range. More importantly, the resulting PPy nanosheets exhibit prominent in vitro and in vivo photothermal ablation ability toward cancer cells in the NIR II window.

The overall synthetic procedure is schematically illustrated in Figure 1a. To obtain ultrathin PPy nanosheets, a hard template which could confine the growth and assembly of PPy chains is necessary as PPy chains tend to cross-link and form bulk structures under normal synthetic conditions. Iron oxychloride

DOI: 10.1021/acs.nanolett.7b04675
Nano Lett. 2018, 18, 2217−2225

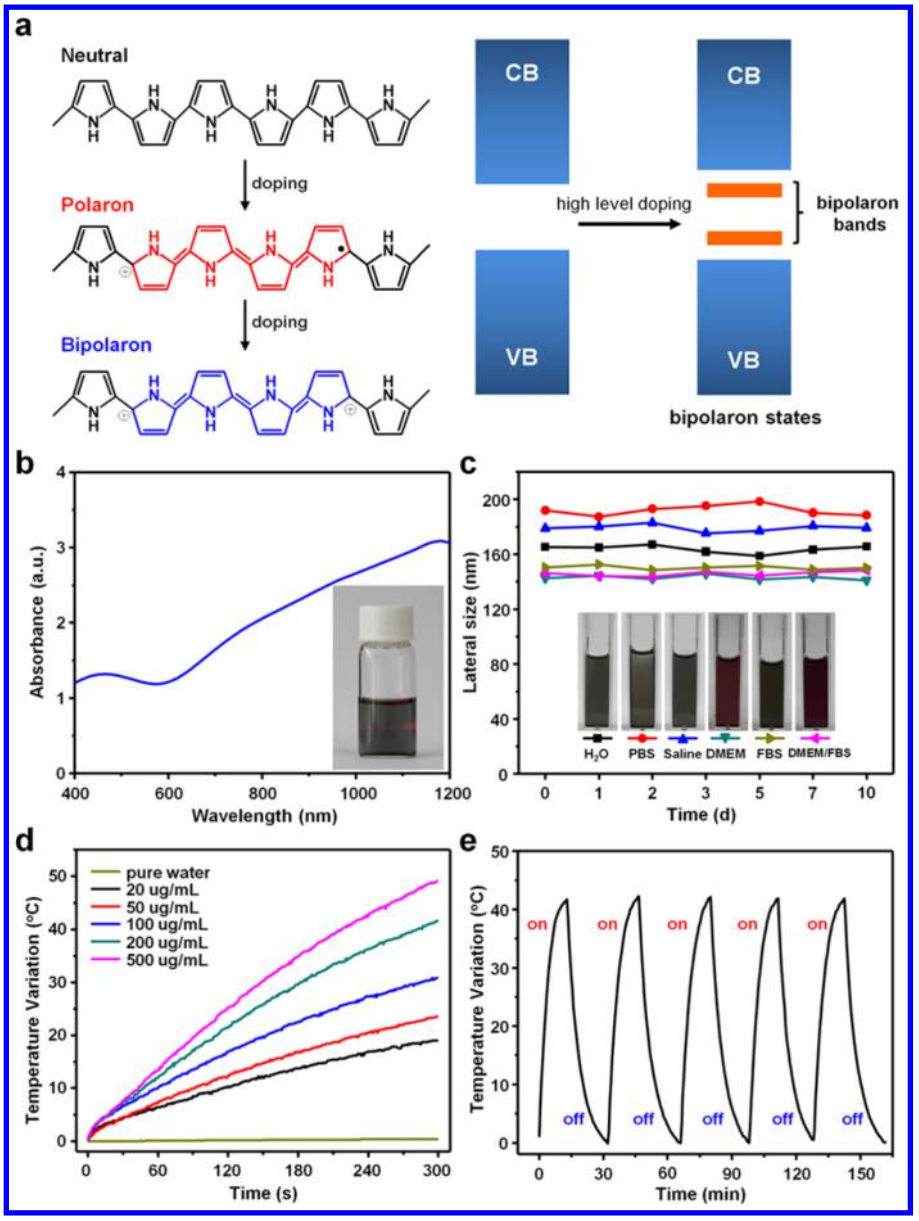

Figure 2. (a) Schematic illustration of the chemical structures and formation of bipolaron bands as a result of increased doping in PPy nanosheets. (b) UV−vis-NIR absorption spectra of PPy nanosheets. (c) DLS profiles of PPy nanosheets coated with DSPE-PEG in different buffer solutions. (d) Photothermal heating curves of ultrathin PPy nanosheets under irradiation of 1064 nm laser (1 W/cm^2). (e) Repeated heating/cooling profiles of aqueous solutions containing PPy nanosheets (100 μg/mL) under irradiation of 1064 nm laser (1 W/cm^2).

(FeOCl), a layered inorganic solid, is an ideal candidate to fulfill the requirement.[45,46] Pyrrole monomers could intercalate into the van der Waals gap in FeOCl followed by in situ polymerization to form PPy thin nanosheets between FeOCl layers.[47] After removing FeOCl template by simple acid washing, ultrathin PPy nanosheets are obtained. This entire process is very convenient and as-obtained PPy nanosheets are stable because PPy chains are cross-linked in the confined 2D space.[48] The FeOCl template was prepared using a chemical vapor transition method. The layered lamellar structure can be clearly revealed by scanning electron microscopy (SEM) (Figure S1). After introducing pyrrole monomers into the template, in situ polymerization occurred and the color of FeOCl turned from brown to black (Figure 1b). As shown in Figure 1c, powder X-ray diffraction (PXRD) measurements clearly show the shift of the (010) peak from 11.4° to 6.9° which corresponds to an increase in FeOCl interlayer spacing from 7.76 to 12.81 Å, indicating the intercalation and formation of PPy chains inside the template.[47] The PXRD results also revealed that removing the FeOCl template via acid washing led to amorphous PPy nanostructures without obvious diffraction peaks (Figure 1c). To obtain PPy nanosheet suitable for biomedical applications, the PPy nanosheets were further purified via centrifugation and filtration.

The structure and morphology of the purified PPy nanosheets were then characterized using transmission electron microscopy (TEM) and atomic force microscopy (AFM), respectively (Figures 1d,e, and S3). Both characterization methods indicated that freestanding PPy nanosheets with lateral sizes around 100−200 nm were obtained. This observation is consistent with the result obtained from dynamic light scattering (DLS) measurement (~123 nm, Figure S2).

DOI: 10.1021/acs.nanolett.7b04675
Nano Lett. 2018, 18, 2217−2225

The thickness of the PPy nanosheets was measured to be around 1−2 nm with slight variations, roughly corresponding to the thickness of single-layer or few-layer PPy nanosheets. The inorganic FeOCl template is relatively rigid and in principle could only yield PPy nanosheets with thickness around ∼1 nm. Thus, the PPy nanosheets with thickness higher than 1 nm are likely caused by the stacking of PPy nanosheets as evidenced by the TEM image shown in Figure S4. The stacking between different nanosheets has been previously observed during TEM or AFM characterization of ultrathin nanosheets.[19,49]

X-ray photoelectron spectroscopy (XPS) measurements were conducted to investigate the surface chemical composition of the ultrathin PPy nanosheets. The survey spectrum revealed the existence of C (68.23 atom %), N (15.79 atom %), O (9.12 atom %), and Cl (6.86 atom %) (Figure S5), indicating that Cl^- ions were doped into the nanosheets at ∼40 mol % doping level. This finding was confirmed by element analysis (EA) which showed that roughly every 2.7 pyrrole units were doped by a Cl^- ion (Table S1). Deconvoluted C 1s peak revealed the presence of C—C (284.8 eV), C═N/C−N^+ (286.3 eV), and C═O (287.9 eV) groups.[50] Meanwhile, the high-resolution N 1s spectrum could be deconvoluted into several peaks at 399.6, 400.6, and 402.5 eV, respectively, implying that charged nitrogen atoms are present in PPy nanosheets. This observation is consistent with previous studies.[51,52] More importantly, this finding can be correlated to nitrogen atoms located outside the bipolarons in the two outer rings of each bipolaron and in the two inner rings of each bipolaron, respectively.[42] Figure 2a explicitly illustrates the variation of chemical structures and formation of the bipolaron bands in PPy nanosheets due to high-level doping.[42,43,53,54] Consequently, the UV−vis-NIR absorption spectrum acquired on the ultrathin PPy nanosheets displayed a unique broadband absorption in NIR region, especially in the NIR II window ranging from 1000 to 1200 nm (Figure 2b). However, spherical PPy nanoparticles with the size around ∼100 nm only exhibited very weak absorbance in the same spectral range (Figure S6), implying that efficient doping in the sheetlike structure is critical for tuning the optical properties of PPy.[40] On the basis of the concentration-dependent UV−vis-NIR absorption, the extinction coefficients at 808 and 1064 nm were measured to be 20.2 and 27.8 L g^{-1} cm^{-1}, respectively (Figure S7). These values are much higher than those of PPy nanoparticles (6.8 L g^{-1} cm^{-1}).[55] Meanwhile, the extinction coefficient at 808 nm is much higher than that of many 2D inorganic counterparts, such as graphene oxide (3.6)[56] and $MoSe_2$ (11.1),[57] and comparable to reduced graphene oxide (24.6),[58] WS_2 (23.8),[59] TiS_2 (26.8),[16] Ta_2NiS_5 (25.6),[60] and Ti_3C_2 (25.2).[19] More importantly, the extinction coefficient at 1064 nm is calculated on the order of 10^{10} M^{-1} cm^{-1}, which is among the highest PTAs in the NIR II window (Table S2).

Additional experiments were conducted to further validate the mechanism illustrated in Figure 2a. Excess amounts of NaOH was first used to dedope the as-synthesized PPy nanosheets. As shown in Figure S8a, the absorption in the NIR II region is dramatically suppressed after dedoping. However, if the dedoped PPy nanosheets were treated with HCl, the absorption in the NIR II region could appear again. More HCl could lead to higher absorption intensity in the NIR II region, indicating that the doping process could control the optical properties of PPy nanosheets. The doping levels (mol %) were determined by EA (Table S4). If different acids such as HNO_3, H_2SO_4, and $HClO_4$ were used to dope the dedoped PPy nanosheets, the absorption of PPy nanosheets in the NIR II region could also recover (Figure S8b). Thus, different dopants could lead to the similar optical properties, further confirming that the unique optical property is induced by doping. Moreover, we also monitored the dedoping and doping processes of PPy nanosheets by adding 1 M NaOH and 1 M HCl into the as-synthesized and dedoped PPy nanosheets solutions, respectively. The UV−vis-NIR absorption spectra are shown in Figure S9. Obviously, the absorption in the NIR II region of the PPy nanosheets gradually decreased by dedoping whereas redoping could gradually induce the recovery of optical absorption in the NIR II region. These in situ dedoping and doping results further validate our conclusion that the unique optical property is caused by doping.

XPS and Raman measurements were employed to correlate the chemical structures of PPy nanosheets to the variations in optical properties as a result of controlled doping and dedoping. After dedoping using excess NaOH, the high-resolution N 1s spectrum of PPy nanosheets can only be deconvoluted into two peaks at 399.6 and 397.5 eV (Figure S10a). This observation is consistent with the structure of neutral PPy nanosheets, implying that the bipolaron band disappeared and the absorption in the NIR II region is suppressed. Raman spectroscopic characterization also revealed critical information on the structures of doped and dedoped PPy nanosheets (Figure S10b). In the Raman spectrum of as-synthesized PPy nanosheets, we observed the bands of C═C in-ring and C—C inter-ring vibrations with a maximum at 1566 cm^{-1}. This peak shifted to 1582 cm^{-1} after dedoping, corresponding to the C═C backbone stretching vibrations in short conjugation length. The peak at 1317 cm^{-1} can be assigned to the C—C ring stretching vibrations of doped PPy which shifted to 1300 cm^{-1} after dedoping. The peak at 1300 cm^{-1} is closely related to the neutral C—C ring stretching vibrations, indicating that neutral PPy formed after dedoping process.[61,62] The peak at 1046 cm^{-1} could be assigned to C—H in-plane vibrations in neutral PPy units. The intensity of this peak increased after dedoping, further suggesting that NaOH treatment could remove dopants from PPy nanosheets to form neutral PPy nanosheets. However, after redoping using HCl, the Raman spectrum could recover, further confirming that the doping and dedoping is a controllable process. Furthermore, to provide more convincing evidence that the 2D ultrathin structure is beneficial for doping, we conducted additional experiments by parallelly doping dedoped PPy nanosheets and PPy nanoparticles under the same conditions. EA and XPS results are shown in Tables S4 and S5. The correlation of doping levels to the amounts of HCl used confirmed that nanosheet structure is beneficial for achieving high doping levels (Figure S11).

Although the as-prepared ultrathin PPy nanosheets can be well dispersed in water without apparent aggregation due to the presence of heavily doped ions, the stability of PPy nanosheets in saline is relatively poor likely due to the "salting out" effect.[63] To improve the stability in physiological conditions, DSPE-PEG was used as the stabilizing agent to prevent the aggregation and enhance the stability of PPy nanosheets in physiological media via van der Waals forces and hydrophobic interactions.[64,65] No dramatic changes can be observed in the UV−vis-NIR spectra (Figure S12) after coating with DSPE-PEG and the lateral size of PPy nanosheets slightly increased to 167 nm (Figure S13). The DSPE-PEG-coated PPy nanosheets exhibit high dispersity in various buffer solutions such as PBS,

DOI: 10.1021/acs.nanolett.7b04675
Nano Lett. 2018, 18, 2217−2225

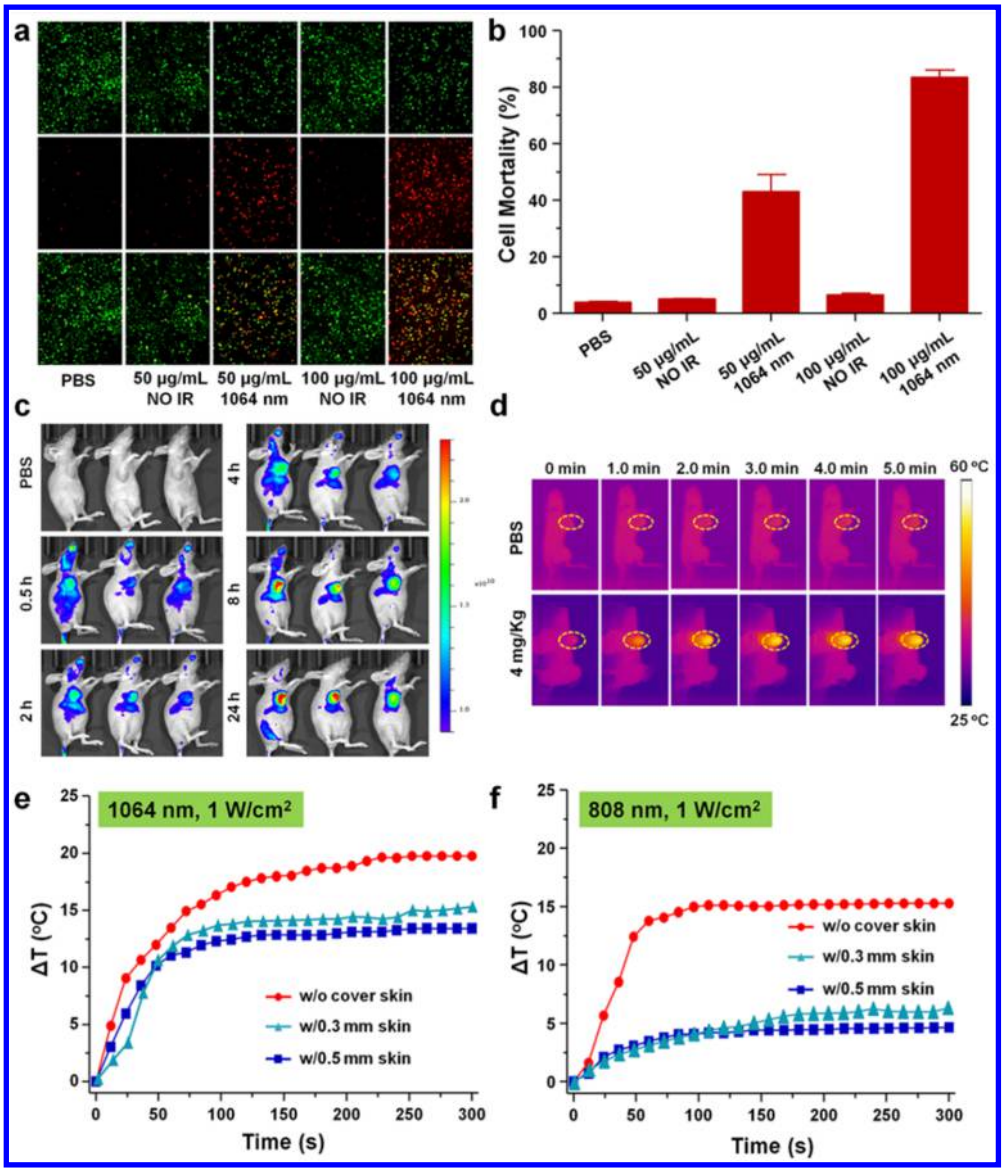

Figure 3. (a) Photothermal destruction of MDA-MB-231 cells with or without PPy nanosheets irradiated with 1064 nm laser (1 W cm^{-2}, 10 min). Live/dead stain for viability shows dead cells as red while viable cells as green. (b) Relative cell mortality of MDA-MB-231 cells after being incubated with different concentrations (50 and 100 μg/mL) of DSPE-PEG coated PPy nanosheets. Error bars were based on the standard deviations (SD) of three parallel samples. (c) DiR fluorescent images at different time points post intravenous injection of DiR loaded PPy nanosheets. (d) IR thermal images of MDA-MB-231 tumor-bearing mice after intravenous injection of PBS and PPy nanosheets using 1064 nm laser (1 W cm^{-2}). (e,f) Temperature evolution in tumors of MDA-MB-231 tumor-bearing mice after intravenous injection of 4 mg kg^{-1} PPy nanosheets upon irradiation with (e) 1064 nm and (f) 808 nm laser (1 W cm^{-2}, 5 min) with or without covered skins.

saline, Dulbecco's modified eagle medium (DMEM), fetal bovine serum (FBS), and DMEM mixed with 10% FBS (Figure 2c). To evaluate the photothermal properties, aqueous solutions containing different concentrations of DSPE-PEG coated PPy nanosheets were irradiated with 1064 nm laser at a power density of 1 W cm^{-2} for 5 min. An obvious concentration-dependent temperature increase was observed for PPy solutions under 1064 nm laser irradiation (Figure 2d). The solution temperature could increase by 49 °C within 5 min irradiation of 1064 nm laser at a concentration of 500 μg mL^{-1}. The temperature could increase by 44 °C under 808 nm laser irradiation (Figure S14). In contrast, the temperature variation for pure water was less than 1 °C under the same condition. Therefore, this result clearly demonstrates the rapid and efficient conversion of NIR energy into thermal energy by the ultrathin PPy nanosheets. The PTCE of ultrathin PPy nanosheets measured by a modified method[66] is as high as 55.6% at 808 nm and this value could even reach 64.6% at 1064 nm (Figure S15), surpassing previous PTAs that are active in the NIR II region (Table S3). The photothermal conversion performance of PPy nanosheets with different doping levels were further investigated under 1064 nm laser irradiation to further validate the doping-induced photothermal effect. Temperature variation profiles and PTCE results are shown in Figure S16. Obviously, dedoped PPy nanosheets only exhibited poor PTCE and increasing the doping level of dedoped PPy nanosheets could lead to higher PTCE.

Photothermal stability is a key parameter for PTT treatment. To assess the photothermal stability of PPy nanosheets coated with DSPE-PEG, the temperature profiles of an aqueous

DOI: 10.1021/acs.nanolett.7b04675
Nano Lett. 2018, 18, 2217−2225

solution containing PPy nanosheets (100 μg mL^{-1}) were recorded for five successive cycles of heating/cooling processes under 1064 nm laser irradiation (Figure 2e). No obvious deterioration could be observed during the repeated cycling tests, implying the potential of PPy nanosheets as durable PTAs for PTT cancer treatment. Meanwhile, negligible change can be observed in the UV−vis-NIR spectra after five successive cycles, indicating the stable photothermal conversion capability of PPy nanosheets (Figure S17).

On the basis of the excellent photothermal properties, especially in the NIR II window, the ultrathin PPy nanosheets were further examined as PTAs for in vitro photothermal cancer therapy in the NIR II window. The biocompatibility of these PPy nanosheets were first evaluated by incubation PPy nanosheets with MDA-MB-231 cells for 24 h. The cell viability was determined using standard MTT assays (Figure S18). No obvious cytotoxicity was observed with DSPE-PEG coated PPy nanosheets up to 400 μg mL^{-1}, which indicates that the PPy nanosheets are highly biocompatible. Subsequently, MDA-MB-231 cells were incubated with DSPE-PEG coated PPy nanosheets at 50 and 100 μg/mL for 2 h and then exposed to 1064 nm laser (1.0 W cm^{-2}, 10 min). Fluorescent live/dead staining was used to differentiate the live (green) and dead (red) cells, respectively, to visualize this photothermal ablation process (Figure 3a). It was revealed that more than 80% of cells were killed for cells treated with 100 μg mL^{-1} PPy nanosheets under 1064 nm laser irradiation (Figure 3b). It is worth mentioning that PPy nanosheets at the same concentration without laser irradiation could not cause obvious toxicity to the cells with cell viability higher than 94% (Figure 3a,b). Thus, in vitro studies clearly demonstrated the remarkable photothermal effect of the PPy nanosheets in promoting cancer cell ablation. Subsequently, we used an in vitro experimental setup to evaluate the NIR tissue penetration performance in the NIR I and NIR II biological windows by detecting photothermal conversion ability of PPy nanosheets using 808 and 1064 nm laser irradiation. In this study, chicken breast muscles with different thicknesses were prepared and used as model biological tissues. A 100 μL solution dispersed DSPE-PEG coated PPy nanosheets covered with the tissues of different thicknesses were subjected to 808 and 1064 nm laser irradiation (1 W cm^{-2}) for 5 min, respectively. The infrared thermographs were then captured by an imaging camera. The measured temperature variations at different thicknesses of the tissues under 808 and 1064 nm laser radiation confirmed that 1064 nm laser exhibited superior tissue penetration capability to the 808 nm laser (Figure S19).

We then investigated the photothermal effect of PPy nanosheets in mice bearing MDA-MB-231 xenograft. 1,1′-Dioctadecyl-3,3,3′,3′-tetramethylindotricarbocyanine iodide (DiR), a NIR dye, was used to track the accumulation of PPy nanosheets in tumors. The lipophilic DiR is highly fluorescent after being incorporated into the hydrophobic DSPE or adsorbed on PPy nanosheets. But the fluorescence is weak once it is released into water. Blood circulation and biodistribution demonstrated an ultralong blood circulation time with a $T_{1/2z}$ of 15.35 h (Figure S20 and Table S6). The tumor-bearing mice was imaged by a Xenogen IVIS spectrum system following systemic administration of DiR-loaded DSPE-PEG coated PPy nanosheets post intravenous injection. As shown in Figures 3c and S21, the fluorescence of DiR in a tumor obviously increased along the time and reached the maximum intensity at 8 h post injection, indicating the effective accumulation of PPy nanosheets in the tumor. The passive accumulation of PPy nanosheets was determined as 6.35% ID/g tissue, attributing to the long blood retention time (Figure S22). Thus, these ultrathin PPy nanosheets are suitable for PTT via intravenous injection. Accordingly, MDA-MB-231 tumor-bearing BALB/c nude mice were intravenously injected with PPy nanosheets at a dose of 4 mg kg^{-1} and the tumors were irradiated with a 1064 nm laser at a density of 1.0 W/cm^2. The temperature increase and spatial temperature distribution at the tumor surface was monitored real-time by an infrared imaging camera. The temperature of the tumor region with PPy nanosheets raised quickly by 20 °C within 4 min whereas the control sample without PPy nanosheets showed negligible increase in temperature (Figure 3d).

Furthermore, NIR II window is more appealing for photothermal treatment of deep buried tumors and PPy nanosheets exhibit better absorbance in the NIR II window. Because our in vitro experiment indicated that the 1064 nm laser exhibited superior tissue penetration capability to the 808 nm laser, the in vivo photothermal performance of PPy nanosheets was assessed using 808 and 1064 nm laser, respectively. As shown in Figure 3e,f, the tumor temperature increased by 20 °C in 4 min using 1064 nm laser whereas the temperature could only increase by 15 °C using 808 nm laser at the same laser power of 1 W cm^{-2}. More importantly, the temperature increase markedly dropped to only 5 °C under 808 nm laser irradiation when the tumor was covered by a 0.3 or 0.5 mm thick mouse skin (Figure 3f). In sharp contrast, the temperature around tumor area could still increase by 14.8 and 13.1 °C under 1064 nm laser irradiation when the tumor was covered by the same mouse skins due to the superior tissue penetration capability of NIR II laser. We also evaluated the in vivo cellular apoptosis inside the tumor at different depths under the skin. Specifically, nude mice with MDA-MB-231 tumor via intravenous administration of DSPE-PEG-coated PPy nanosheets were respectively treated under 808 and 1064 nm laser irradiation (Figure S23a). After photothermal treatments, the mice were sacrificed and tumor tissues were excised, fixed in 4% formaldehyde, and embedded in paraffin. Then, paraffin-embedded 5 μm tumor sections were obtained and dissected to observe the cellular apoptosis at different depths inside the tumor tissues. Immunnohistochemical staining of the terminal transferase dUTP nick-end labeling (TUNEL) assay revealed that the effective photothermal ablation of orthotopic xenograft tumors in nude mice could be achieved at the depth of ∼8 and ∼6 mm using 1064 and 808 nm laser, respectively (Figure S23b,c). This experiment clearly indicates the great promise of using PPy nanosheets for deep tissue photothermal therapy in NIR II window. Therefore, our study clearly suggests the great promise of using ultrathin PPy nanosheets for deep tissue PTT in NIR II window.

Encouraged by the above photothermal results and the deep tissue penetration of light in the NIR II window, we next studied in vivo therapeutic efficacy of PTT using PPy nanosheets following systemic administration. MDA-MB-231 tumor-bearing mice were divided into six groups with five mice per group. Tumors of every group were intravenous injected with 50 μL PPy solution (dose = 4 mg kg^{-1}) and irradiated by the 808 and 1064 nm laser (1 W cm^{-2}) with or without 0.5 mm skin, respectively. The tumor sizes of all groups were measured by a caliper every third day after treatment. Obviously, 1064 nm laser was more effective in PTT compared to the 808 nm laser (Figure 4a−c). The tumors treated with PPy nanosheets under

DOI: 10.1021/acs.nanolett.7b04675
Nano Lett. 2018, 18, 2217−2225

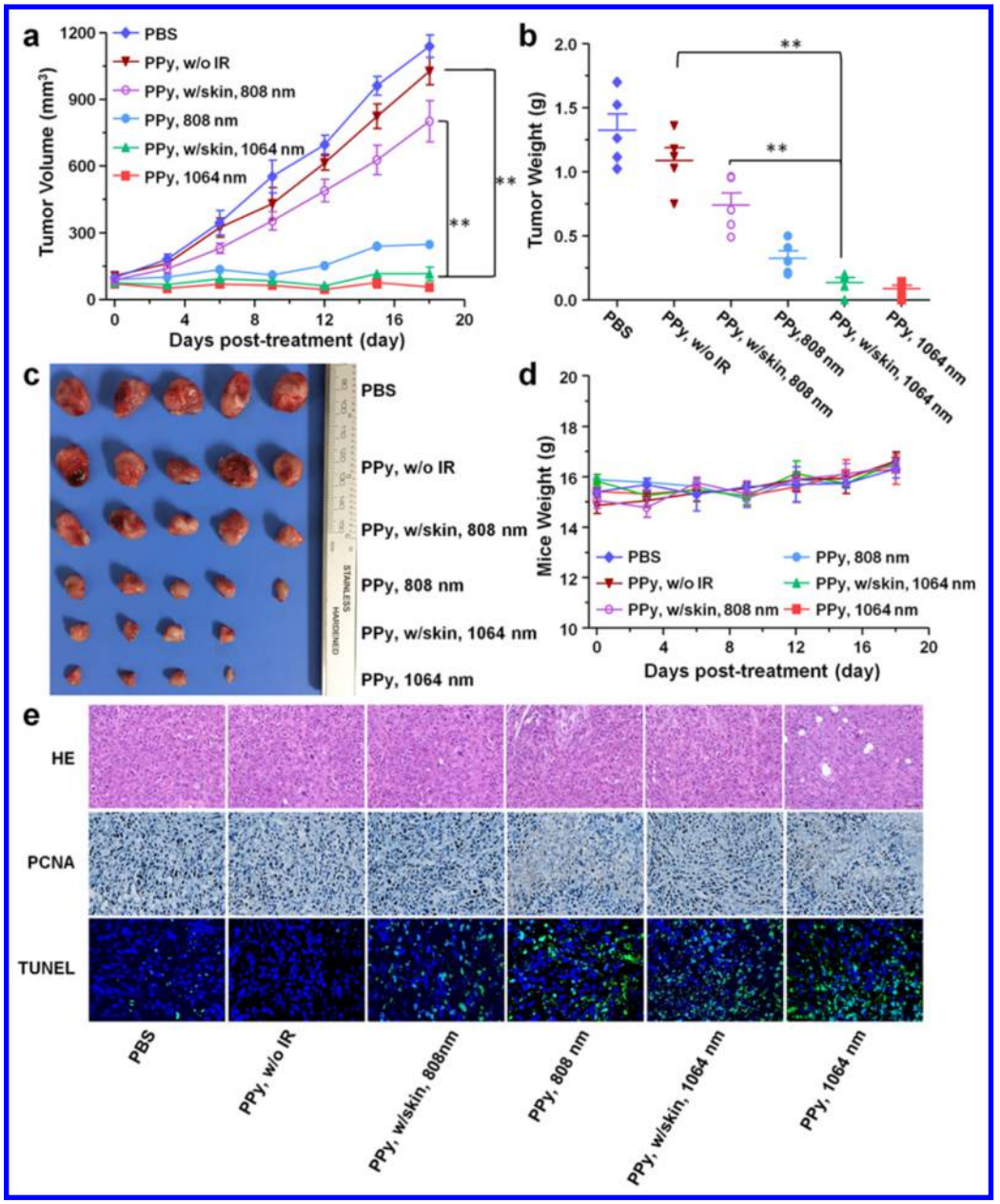

Figure 4. MDA-MB-231 tumor (a) growth curves, (b) tumor weight, and (c) tumor images of various groups after intravenous injection of different samples using different laser irradiation conditions (1 W cm^{-2}, 10 min). (d) Body weights of mice bearing MDA-MB-231 breast cancer xenografts at different time points after treatment with the above formulations. (e) H&E, PCNA, and TUNEL analyses of tumor tissues at the last time point of the treatment (scale bar = 50 μm). The brown cells represent the PCNA-positive proliferating cells and the green cells represent the TUNEL-positive apoptotic cells.

1064 nm laser irradiation were effectively ablated. However, the tumors treated with PPy nanosheets under 808 nm irradiation was less effective. This phenomenon was more apparent when the tumor was cover by a 0.5 mm skin, indicating NIR II window is more effective for penetrating tissues and treating deep buried tumors. Meanwhile, the tumors weight (Figure 4b), tumors image (Figure 4c), and mice weight (Figure 4d) further verified that PPy nanosheets exhibited excellent photothermal effect to enhance tumor thermal ablation without causing significant cytotoxicity to the mice. Haematoxylin & eosin (H&E) staining of tumor slices was carried out for tumors collected immediately after mice were sacrificed. At the same time, cell proliferation and apoptosis of tumor tissues were also analyzed by PCNA and TUNEL analyses (Figure 4e). As expected, significant tumor cell damage (H&E), effectively reduced the percentage of proliferating tumor cells (PCNA) and increased the percentage of tumor cells undergoing apoptosis (TUNEL), was noticed in the tumor with PPy nanosheets. In our in vivo photothermal study, no significant body weight drop was observed (Figure 4d), implying that PPy nanosheets are not toxic to the treated animals. H&E stained images of major organs showed no noticeable damages in all major organs of mice 18 days after PTT treatment, confirming that PPy nanosheets are highly biocompatible (Figure S24). In addition, the PPy nanosheets are constructed by pyrrole units via covalent C—C bonds, suggesting that they are very difficult to be degraded in vivo like other carbon nanomaterials. Because PPy nanosheets structurally resemble graphene and they

DOI: 10.1021/acs.nanolett.7b04675
Nano Lett. 2018, 18, 2217−2225

primarily accumulate in reticuloendothelial system organs (Figure S22), we speculate that PPy nanosheets may be excreted via both fecal and renal clearance as revealed in chemically functionalized graphenes.[67,68] Thus, our results suggest that PPy nanosheets are very promising PTAs for in vivo tumor photothermal therapeutics.

To further exemplify the advantages of using the ultrathin PPy nanosheets for photothermal therapy in the NIR II window, we investigated the in vivo therapeutic efficacy of PPy nanosheets in parallel with RGOPAA composite and Au@$Cu_{2-x}S$ nanorods.[25,31] Both control samples were reported to be active in the NIR II widow. As shown in Figure S25, the tumors injected with PPy nanosheets were much smaller compared to those injected with RGOPAA composite and Au@$Cu_{2-x}S$ nanorods. The tumors treated with PPy nanosheets under 1064 nm laser irradiation were effectively ablated because of the higher PTCE of PPy nanosheets, whereas the tumors treated with RGOPAA composite and Au@$Cu_{2-x}S$ nanorods under the same 1064 nm irradiation were less effective. The results from this parallel in vivo photothermal test provide convincing evidence that the ultrathin PPy nanosheets are very promising for photothermal therapy in the NIR II window.

In conclusion, we for the first time demonstrated a novel 2D polymer-based PTA for high-performance photothermal therapeutics in the NIR II window. Ultrathin PPy nanosheets were prepared via a space-confined synthesis method using layered FeOCl as the removable template. The ultrathin PPy nanosheets possess a strong NIR absorbance in the NIR II window due to the formation of bipolaron band. The bipolaron band is formed without using additional doping sources. The resulting PPy nanosheets also exhibited superior photothermal conversion efficiency to previous PTAs in the NIR II window. This character is significant as it could provide a new platform allowing for deeper penetration depth and higher maximum permissible exposure in PTT. Both in vitro and in vivo photothermal studies demonstrate that ultrathin PPy nanosheets could serve as excellent PTAs for photothermal ablation of cancer cells. Our study not only promises the great potential of PPy nanosheets as a novel agent for cancer therapy but may also lead to explore more polymer nanostructures for biomedical applications.

■ ASSOCIATED CONTENT

Supporting Information

The Supporting Information is available free of charge on the ACS Publications website at DOI: 10.1021/acs.nanolett.7b04675.

Synthetic and experimental details, additional SEM and AFM images, UV/vis absorption spectra, photothermal results, DLS profiles, cytotoxicity assessment, and DiR fluorescence analysis (PDF)

■ AUTHOR INFORMATION

Corresponding Authors

*E-mail: hxu@ustc.edu.cn (H.X.).
*E-mail: yucaiwang@ustc.edu.cn (Y.W.).

ORCID

Yucai Wang: 0000-0001-6046-2934
Hangxun Xu: 0000-0003-1645-9003

Author Contributions

X.W. and Y.M. contributed equally to this work. H.X. and Y.W. conceived the project. X.W. performed the synthesis, characterization, and photothermal tests. Y.M. performed in vitro and in vivo photothermal studies.

Notes

The authors declare no competing financial interest.

■ ACKNOWLEDGMENTS

This work is supported by the MOST (2015CB351903, 2017YFA0207301), National Natural Science Foundation of China (21474095, 51573176, and 51633008), CAS Key Research Program of Frontier Sciences (QYZDB-SSW-SLH018), and the Fundamental Research Funds for the Central Universities.

■ REFERENCES

(1) Cheng, L.; Wang, C.; Feng, L.; Yang, K.; Liu, Z. *Chem. Rev.* **2014**, *114*, 10869−10939.
(2) Melancon, M. P.; Zhou, M.; Li, C. *Acc. Chem. Res.* **2011**, *44*, 947−956.
(3) Jaque, D.; Maestro, L. M.; del Rosal, B.; Gonzalez, P. H.; Benayas, A.; Plaza, J. L.; Rodriguez, E. M.; Sole, J. G. *Nanoscale* **2014**, *6*, 9494−9530.
(4) Wang, W.; Wang, L.; Li, Y.; Liu, S.; Xie, Z.; Jing, X. *Adv. Mater.* **2016**, *28*, 9320−9325.
(5) Taratula, O.; Schumann, C.; Duong, T.; Taylor, K. L.; Taratula, O. *Nanoscale* **2015**, *7*, 3888−3902.
(6) Chandra, A.; Deshpande, S.; Shinde, D. B.; Pillai, V. K.; Singh, N. *ACS Macro Lett.* **2014**, *3*, 1064−1068.
(7) Abbas, M.; Zou, Q.; Li, S.; Yan, X. *Adv. Mater.* **2017**, *29*, 1605021.
(8) Espinosa, A.; Di Corato, R.; Kolosnjaj-Tabi, J.; Flaud, P.; Pellegrino, T.; Wilhelm, C. *ACS Nano* **2016**, *10*, 2436−2446.
(9) Barhoumi, A.; Wang, W.; Zurakowski, D.; Langer, R. S.; Kohane, D. S. *Nano Lett.* **2014**, *14*, 3697−3701.
(10) Rengan, A. K.; Bukhari, A. B.; Pradhan, A.; Malhotra; Banerjee, R.; Srivastava, R.; De, A. *Nano Lett.* **2015**, *15*, 842−848.
(11) Kurapati, R.; Kostarelos, R.; Prato, M.; Bianco, A. *Adv. Mater.* **2016**, *28*, 6052−6074.
(12) Li, R.; Zhang, L.; Shi, L.; Wang, P. *ACS Nano* **2017**, *11*, 3752−3759.
(13) Chen, Y.; Tan, C.; Zhang, H.; Wang, L. *Chem. Soc. Rev.* **2015**, *44*, 2681−2701.
(14) Yang, K.; Hu, L.; Ma, X.; Ye, S.; Cheng, L.; Shi, X.; Li, C.; Li, Y.; Liu, Z. *Adv. Mater.* **2012**, *24*, 1868−1872.
(15) Chimene, D.; Alge, D. L.; Gaharwar, A. K. *Adv. Mater.* **2015**, *27*, 7261−7284.
(16) Qian, X.; Shen, S.; Liu, T.; Cheng, T.; Liu, Z. *Nanoscale* **2015**, *7*, 6380−6387.
(17) Yin, W.; Yan, L.; Yu, J.; Tian, G.; Zhou, L.; Zheng, X.; Zhang, X.; Yong, Y.; Li, J.; Gu, Z.; Zhao, Y. *ACS Nano* **2014**, *8*, 6922−6933.
(18) Shao, J.; Xie, H.; Huang, H.; Li, Z.; Sun, Z.; Xu, Y.; Xiao, Q.; Yu, X.; Zhao, Y.; Zhang, H.; Wang, H.; Chu, P. K. *Nat. Commun.* **2016**, *7*, 12967.
(19) Lin, H.; Gao, S.; Dai, C.; Chen, Y.; Shi, J. *J. Am. Chem. Soc.* **2017**, *139*, 16235−16247.
(20) Zhao, Z.; Shi, S.; Huang, Y.; Tang, S.; Chen, X. *ACS Appl. Mater. Interfaces* **2014**, *6*, 8878−8885.
(21) Chen, Y.; Wang, L.; Shi, J. *Nano Today* **2016**, *11*, 292−308.
(22) Ding, X.; Chi, H.; Zhang, M.; Huang, R.; Li, C.; Shen, H.; Liu, M.; Zou, Y.; Gao, N.; Zhang, Z.; Li, Y.; Wang, Q.; Li, S.; Jiang, J. *J. Am. Chem. Soc.* **2014**, *136*, 15684−15693.
(23) Bashkatov, A. N.; Genina, E. A.; Kochubey, V. I.; Tuchin, V. V. J. *J. Phys. D: Appl. Phys.* **2005**, *38*, 2543.
(24) Li, A.; Li, X.; Yu, X.; Li, W.; Zhao, R.; An, X.; Cui, D.; Chen, X.; Li, W. *Biomaterials* **2017**, *112*, 164−175.
(25) Ji, M.; Zhang, W.; Yang, Z.; Huang, L.; Liu, J.; Zhang, Y.; Gu, L.; Yu, Y.; Hao, W.; An, P.; Zheng, L.; Zhu, H.; Zhang, J.; et al. *Adv. Mater.* **2016**, *28*, 3094−3101.

DOI: 10.1021/acs.nanolett.7b04675
Nano Lett. 2018, 18, 2217−2225

(26) Park, J. E.; Kim, M.; Hwang, J. H.; Nam, J. M. *Small Methods* **2017**, *1*, 1600032.
(27) Vijayaraghavan, P.; Liu, C.; Vankayala, R.; Chiang, C.; Hwang, K. C. *Adv. Mater.* **2014**, *26*, 6689−6695.
(28) Tsai, M.; Chang, S. G.; Cheng, F.; Shanmugam, V.; Cheng, Y.; Su, C.; Yeh, C. *ACS Nano* **2013**, *7*, 5330−5342.
(29) Zhang, Q.; Ge, J.; Pham, T.; Goebl, J.; Hu, Y.; Lu, Z.; Yin, Y. *Angew. Chem., Int. Ed.* **2009**, *48*, 3516−3519.
(30) Maestro, L. M.; Haro-Gonzalez, P.; del Rosal, B.; Ramiro, J.; Caamano, A. J.; Carrasco, E.; Juarranz, A.; Sanz-Rodriguez, F.; Sole, J. G.; Jaque, D. *Nanoscale* **2013**, *5*, 7882−7889.
(31) Sinha, M.; Gollavelli, G.; Ling, Y. *RSC Adv.* **2016**, *6*, 63859−63866.
(32) Cao, Y.; Dou, J.; Zhao, N.; Zhang, S.; Zheng, Y.; Zhang, J.; Wang, J.; Pei, J.; Wang, Y. *Chem. Mater.* **2017**, *29*, 718−725.
(33) Wang, X.; Li, H.; Liu, X.; Tian, Y.; Guo, H.; Jiang, T.; Luo, Z.; Jin, K.; Kuai, X.; Liu, Y.; Pang, Z.; Yang, W.; Shen, S. *Biomaterials* **2017**, *143*, 130−141.
(34) Peng, Z.; Qin, J.; Li, B.; Ye, K.; Zhang, Y.; Yang, X.; Yuan, F.; Huang, L.; Hu, J.; Lu, X. *Nanoscale* **2015**, *7*, 7682−7691.
(35) Hu, P.; Han, L.; Dong, S. *ACS Appl. Mater. Interfaces* **2014**, *6*, 500−506.
(36) Tian, Y.; Zhang, J.; Tang, S.; Zhou, L.; Yang, W. *Small* **2016**, *12*, 721−726.
(37) Ke, K.; Lin, L.; Liang, H.; Chen, X.; Han, C.; Li, J.; Yang, H. *Chem. Commun.* **2015**, *51*, 6800−6803.
(38) Yang, Z.; Ren, J.; Ye, Z.; Zhu, W.; Xiao, L.; Zhang, L.; He, Q.; Xu, Z.; Xu, H. *J. Mater. Chem. B* **2017**, *5*, 1108−1116.
(39) Chen, M.; Fang, X.; Tang, S.; Zheng, N. *Chem. Commun.* **2012**, *48*, 8934−8936.
(40) Xiao, Z.; Peng, C.; Jiang, X.; Peng, Y.; Huang, X.; Guan, G.; Zhang, W.; Liu, X.; Qin, Z.; Hu, J. *Nanoscale* **2016**, *8*, 12917−12928.
(41) Li, Y. *Organic Optoelectronic Materials*; Springer International Publishing, 2015.
(42) Bredas, J. L.; Scott, J. C.; Yakushi, K.; Street, G. B. *Phys. Rev. B: Condens. Matter Mater. Phys.* **1984**, *30*, 1023−1025.
(43) Yang, R.; Smyrl, W. H.; Evans, D. F.; Hendrickson, W. A. *J. Phys. Chem.* **1992**, *96*, 1428−1430.
(44) Cabala, R.; Skarda, J.; Potje-Kamloth, K. *Phys. Chem. Chem. Phys.* **2000**, *2*, 3283−3291.
(45) Wu, C. G.; DeGroot, D. C.; Marcy, H. O.; Schindler, J. L.; Kannewurf, C. R.; Bakas, T.; Papaefthymiou, V.; Hirpo, W.; Yesinowski, J. P.; Liu, Y. J.; Kanatzidis, M. G. *J. Am. Chem. Soc.* **1995**, *117*, 9229−9242.
(46) Kanatzidis, M. G.; Wu, C. G.; Marcy, H. O.; DeGroot, D. C.; Kannewurf, C. R.; Kostikas, A.; Papaefthymiou, V. *Adv. Mater.* **1990**, *2*, 364−366.
(47) Kanatzidis, M. G.; Tonge, L. M.; Marcy, H. O.; Marks, T. J.; Kannewurf, C. R. *J. Am. Chem. Soc.* **1987**, *109*, 3797−3799.
(48) Yanai, N.; Uemura, T.; Ohba, M.; Kadowaki, Y.; Maesato, M.; Takenaka, M.; Nishitsuji, S.; Hasegawa, H.; Kitagawa, S. *Angew. Chem., Int. Ed.* **2008**, *47*, 9883−9886.
(49) Tan, C.; Zhang, H. *Nat. Commun.* **2015**, *6*, 7873.
(50) Malitesta, C.; Losito, I.; Sabbatini, L.; Zambonin, P. G. *J. Electron Spectrosc. Relat. Phenom.* **1995**, *76*, 629−634.
(51) Pfluger, P.; Street, G. B. *J. Chem. Phys.* **1984**, *80*, 544−553.
(52) Plfuger, P.; Krounbi, M.; Street, G. B.; et al. *J. Chem. Phys.* **1983**, *78*, 3212−3218.
(53) Hu, Y.; Yang, R.; Evans, D. F.; Weaver, J. H. *Phys. Rev. B: Condens. Matter Mater. Phys.* **1991**, *44*, 13660−13665.
(54) Bredas, J. L.; Street, G. B. *Acc. Chem. Res.* **1985**, *18*, 309−315.
(55) Wang, Q.; Wang, J.; Lv, G.; Wang, F.; Zhou, X.; Hu, J.; Wang, Q. *J. Mater. Sci.* **2014**, *49*, 3484−3490.
(56) Zhang, S.; Sun, C.; Zeng, J.; Sun, Q.; Wang, G.; Wang, Y.; Wu, Y.; Dou, S.; Gao, M.; Li, Z. *Adv. Mater.* **2016**, *28*, 8927−8936.
(57) Lei, Z.; Zhu, W.; Xu, S.; Ding, J.; Wan, J.; Wu, P. *ACS Appl. Mater. Interfaces* **2016**, *8*, 20900−20908.
(58) Robinson, J. T.; Tabakman, S. M.; Liang, Y.; Wang, H.; Casalongue, H. S.; Vinh, D.; Dai, H. *J. Am. Chem. Soc.* **2011**, *133*, 6825−6831.
(59) Cheng, L.; Liu, J.; Gu, X.; Gong, H.; Shi, X.; Liu, T.; Wang, C.; Wang, X.; Liu, G.; Xing, H.; Bu, W.; Sun, B.; Liu, Z. *Adv. Mater.* **2014**, *26*, 1886−1893.
(60) Zhu, H.; Lai, Z.; Zhen, X.; Tan, C.; Qi, X.; Ding, D.; Chen, P.; Zhang, H.; Pu, K.; et al. *Small* **2017**, *13*, 1604139.
(61) Crowley, K.; Cassidy, J. *J. Electroanal. Chem.* **2003**, *547*, 75−82.
(62) Liu, Y. *J. Electroanal. Chem.* **2004**, *571*, 255−264.
(63) Tan, C.; Zhao, L.; Yu, P.; Huang, Y.; Chen, B.; Lai, Z.; Qi, X.; Goh, M. H.; Zhang, X.; Han, S.; Wu, X. J.; Liu, Z.; Zhao, Y.; Zhang, H. *Angew. Chem.* **2017**, *129*, 7950−7954.
(64) Tao, W.; Ji, X.; Islam, M. A.; Li, Z.; Chen, Si.; Saw, P. E.; Zhang, H.; Bharwani, Z.; Guo, Z.; Shi, J.; Farokhzad, O. C.; et al. *Angew. Chem., Int. Ed.* **2017**, *56*, 11896−11900.
(65) Liu, Z.; Tabakman, S.; Welsher, K.; Dai, H. *Nano Res.* **2009**, *2*, 85−120.
(66) Roper, D. K.; Ahn, W.; Hoepfner, M. *J. Phys. Chem. C* **2007**, *111*, 3636−3641.
(67) Yang, H.; Wan, J.; Zhang, S.; Zhang, Y.; Lee, S. T.; Liu, Z. *ACS Nano* **2011**, *5*, 516−522.
(68) Jasim, D. A.; Ménard-Moyon, C. M.; Begin, D.; Bianco, A.; Kostarelos, K. *Chem. Sci.* **2015**, *6*, 3952−3964.

DOI: 10.1021/acs.nanolett.7b04675
Nano Lett. 2018, 18, 2217−2225